Electronic structure and x-ray-absorption near-edge structure of amorphous Zr-oxide and Hf-oxide thin films: A first-principles study

SungKwan Kim,[a] Yangsoo Kim, and Jongin Hong
Department of Materials Science and Engineering, Korea Advanced Institute of Science and Technology, Daejeon 305701 Korea

Isao Tanaka
Department of Energy Science and Technology, Kyoto University, Kyoto 606-01, Japan

Kwangsoo No
Department of Materials Science and Engineering, Korea Advanced Institute of Science and Technology, Daejeon 305701, Korea

(Received 16 June 2004; accepted 10 February 2005; published online 28 March 2005)

First-principles calculations were performed on the electronic structure and x-ray-absorption near-edge structure (XANES) of amorphous Zr-oxide and Hf-oxide thin films. Using the discrete variational X-α method, the authors simulated the films with $(Zr_4O_{17})^{-18}$ and $(Hf_4O_{18})^{-20}$ clusters. The O–Zr and O–Hf bonds were found to have different characteristics along the bond orientation. By comparing the experimental and calculated XANES, we analyze the absorption mechanism of amorphous Zr-oxide and Hf-oxide thin films for energies up to 10 eV above the O K edge. © *2005 American Institute of Physics*. [DOI: 10.1063/1.1884268]

I. INTRODUCTION

Transition-metal (TM) oxide thin films such as Zr-oxide and Hf-oxide thin films have recently attracted interest because of their unique properties, particularly their high dielectric constant, relatively large band gap, and stability. Given their high dielectric properties, these films were investigated as a potential replacement dielectric to reduce the tunneling current through the gate oxide of a field-effect transistor[1,2] (FET). In the lithographic process, TM oxides have also been considered as a substitute for the phase-shift mask because of their optical properties. In deep ultraviolet (DUV) lithography, the phase-shift masks (PSM) of Cr compounds and MoSiON have a low refractive index of less than 2.5. As a result, the thickness of the PSM that satisfies the requirements of transmittance and phase shift is greater than 90 nm.[3,4] This thickness causes an error when patterns are formed on a wafer, TM oxides with a high dielectric constant can reduce the error.

To calculate the electronic structure and the x-ray-absorption near-edge structure (XANES) of amorphous Zr-oxide and Hf-oxide thin films, we used density-functional theory (DFT) with the X-α approximation,[5,6] and the generalized gradient approximation.[7] XANES spectroscopy is a powerful technique for probing empty states in solids. We therefore used it to investigate the unoccupied partial density of states (PDOS) of the probed atom. One advantage of XANES spectroscopy is that it uses an electric-dipole transition in the core-loss process to excite an electron from a core level to an unoccupied state. To investigate the optical properties of amorphous Zr-oxide and Hf-oxide thin films, we used the electronic structure analysis and XANES spectroscopy.

[a]Electronic mail: ksgyon@kaist.ac.kr

II. EXPERIMENTAL PROCEDURE

To fabricate the amorphous Zr-oxide and Hf-oxide films, we used rf magnetron sputtering under various conditions of deposition power (80, 160, 240, and 320 W), gas-flow rate [Ar:20 sccm (sccm denotes cubic centimeter per minute at STP) and O_2: 1 sccm], pressure (10 mTorr), and time (130 min). To calculate the optical band gaps, we used the Tauc rule.[8]

$$(\alpha\hbar\omega)^{1/2} = \text{const}\ (\hbar\omega - E_g)$$
$$\alpha = 2.303 \times \frac{\log(I_0/I)}{d}(\text{cm}^{-1}), \tag{1}$$

where α is the absorption coefficient, $\hbar\omega$ is the photon energy, $\log(I_0/I)$ is the absorbance, and d is the film thickness. The x-ray diffraction confirmed the crystallization of Zr- and Hf-oxide films deposited above 140 W. Here, plasma bombardment caused the substrate temperature to rise from 60 to 125 °C. The analysis of the optical band gaps and x-ray diffraction confirmed that the optical band gaps are 4.37 eV for the amorphous Zr-oxide thin film and 4.44 eV for the amorphous Hf-oxide thin film.

To calculate the electronic structures and the O K edge of amorphous Zr-oxide and Hf-oxide thin films, we use a program SCAT based on the discrete variational $X\alpha$ (DV-$X\alpha$) method,[5,6] and the program WIEN2K,[9] based on the full-potential, linearized, augmented-plane-wave (FLAPW) methods and the generalized gradient approximation for exchange and correlation.[7]

III. RESULTS AND DISCUSSION

For the SCAT program, amorphous Zr-oxide and Hf-oxide thin films are modeled based on a monoclinic phase of Zr oxide and Hf oxide by introducing oxygen defects to

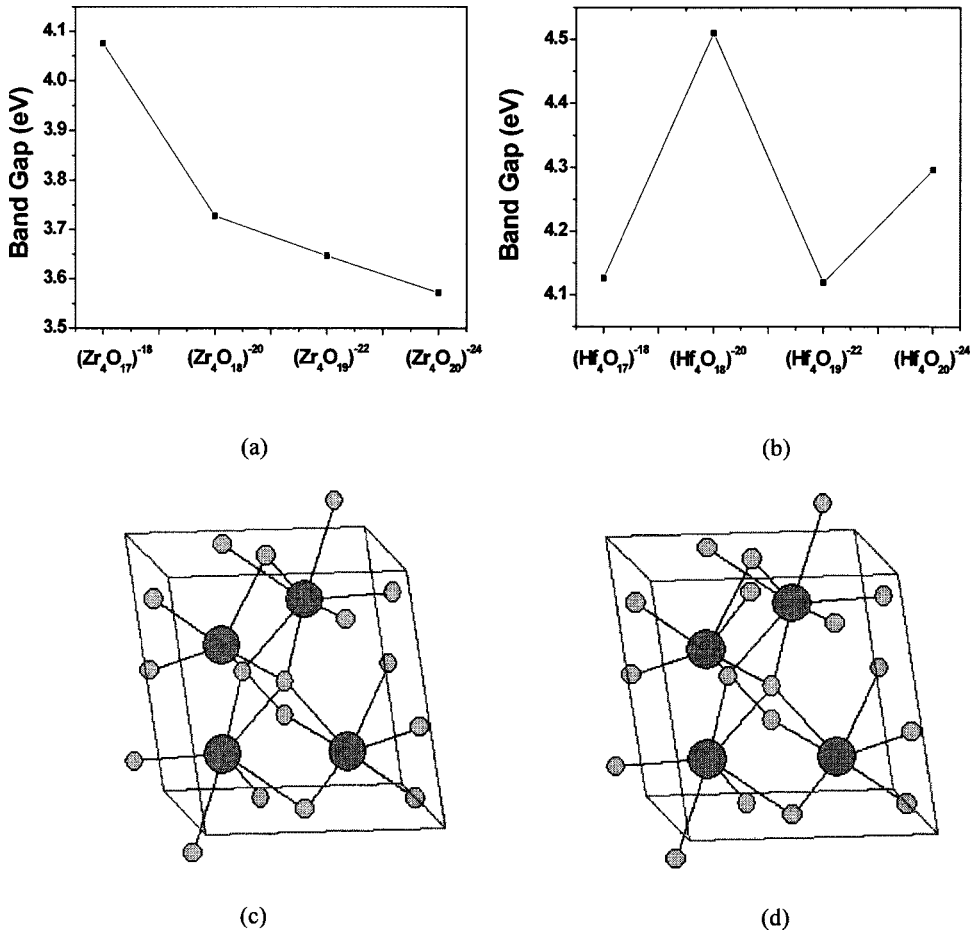

FIG. 1. Band-gap variations of cluster models of an amorphous Zr-oxide thin film (a) and of an amorphous Hf-oxide thin film (b); Models for (a) amorphous Zr-oxide thin films $[(Zr_4O_{17})^{-18}]$ and (b) amorphous Hf-oxide thin films $[(Hf_4O_{18})^{-20}]$.

find out the appropriate cluster models for amorphous Zr- and Hf-oxide thin films, respectively. Oxygen defects are created considering the overlap population between oxygen and Zr (and Hf) and the net charge. Figures 1(a) and 1(b) show the band-gap variations of four cluster models considering the oxygen defects. Cluster models of $(Zr_4O_{17})^{-18}$ [Fig. 1(c)] and $(Hf_4O_{18})^{-20}$ [Fig. 1(d)] have similar band gaps [4.07 eV for $(Zr_4O_{17})^{-18}$ and 4.50 eV for $(Hf_4O_{18})^{-20}$] as the experimental optical band gaps. (−18 and −20 in the cluster models are the total charge of each cluster.) In each model, the oxygen atom for the corresponding core loss is placed at the center of the cluster models. Each cluster is embedded in point charges located at the external atomic sites so as to produce an effective Madelung potential. Each cluster has two different Zr or Hf atom sites around O atom according to the bonding environment. In the electron-energy-loss process, an electron is promoted from a core level to an unoccupied state leaving a core hole. To reproduce the experimental spectrum, self-consistent calculation should be carried out including a core hole. The difference in total energies between initial and final states (transition energy) is well approximated as the difference in molecular-orbital (MO) energies calculated for the Slater transition state where half of an electron is removed from a core orbital and put into an unoccupied MO.[10]

For a WIEN2K,[7,8] the supercell calculations are done for a $2\times2\times1$ supercell containing 48 atoms. Each supercell for amorphous Zr-oxide and Hf-oxide thin films is modeled based on models for the SCAT program. In this calculation, the potentials are described by two kinds of basis sets: inside the nonoverlapping atomic spheres, a linear combination of radial functions times a spherical harmonics was used; in the interstitial region, a plane-wave function was used. The energy-loss near-edge structure (ELNES) calculation is achieved using supercells and one full core hole for the comparison of calculation results.[11]

Figures 2(a) and (b) show the density of states, including the partial density of states (PDOS) of each atomic level, and the bond-overlap population diagrams for two models (Fig. 1(c) and (d) The lower band of the amorphous Zr-oxide thin film, which occurs between −18 and −13 eV, is mainly comprised of O 2*s* states, but is partially hybridized with Zr 4*p* states. The two peaks denoted by *a*1 and *b*2 occur in the lower band according to the interaction of O and Zr. Peak *a* and *b* signifies bonding; peak *b*, antibonding. Furthermore, the notation of 1 and 2 on peak *a* and *b* are related to the distinct Zr sites denoted by Zr^1 and Zr^2; that is, the bonding of O 2*s* and Zr^1 4*p* causes peak *a*1. The upper band that ranges from −7.5 to 1.39 eV is mainly comprised of O 2*p* and Zr 4*d* states. It has three peaks (*c*1, *c*12, and *d*12) that are related to the bonding of O 2*p* and the antibonding of Zr 4*d*. Peak *c* signifies bonding; peak *d*, antibonding. O 2*p*–Zr 4*d* hybridization contributes to the upper band and makes a relatively large contribution to the bonding in amorphous Zr-oxide thin films. The calculated net charges are −1.32 for O, 3.02 for Zr^1, and 3.15 for Zr^2. The bond-overlap

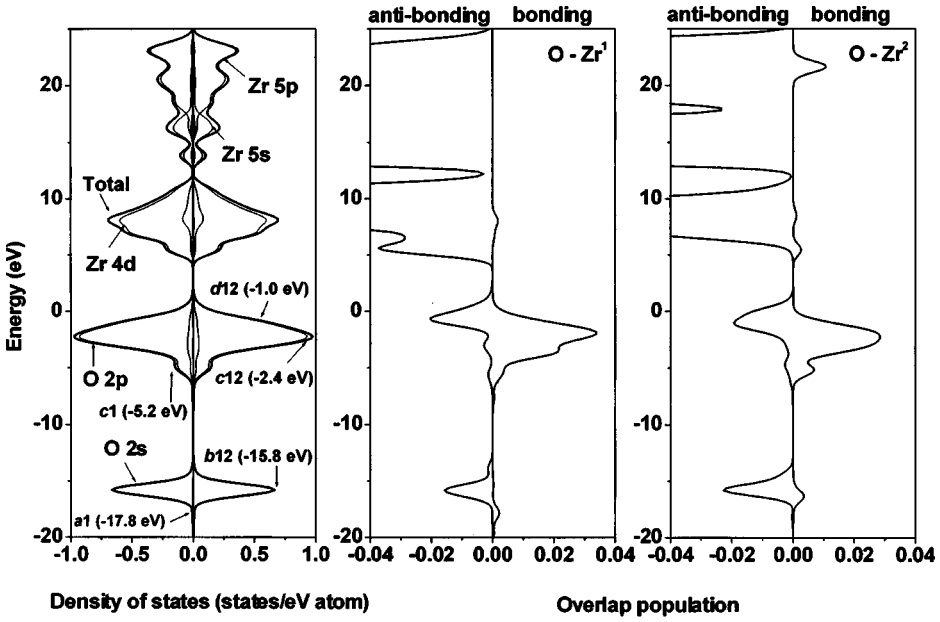

FIG. 2. Total spin density of states and bond-overlap population diagrams for (a) $[(Zr_4O_{17})^{-18}]$ and (b) $(Hf_4O_{18})^{-20}$.

populations are 0.043 for the O–Zr^1 bond and 0.025 for the O–Zr^2 bond. The O–Zr^1 bond has relatively strong covalence, and the O–Zr^2 bond has a relatively strong ionic characteristic. These characteristics suggest that the Zr-oxide thin film has a mixture of ionic and covalent bonding character.

The lower band of the amorphous Hf-oxide thin film, which ranges from −18.2 to −14.2 eV, is composed mainly of O 2*s* and Hf 5*p* states. Moreover, Hf 4*f*, 5*d* states partially make up the lower band. The lower band has two peaks (*e*1 and *f*12). Peak *e* signifies bonding; peak *f*, antibonding. The numbers "1" and "2" in the peak refer to the distinct Hf sites of Hf^1 and Hf^2. The upper band of the Hf-oxide thin film, lying from −7.8 to 1.72 eV, is mainly composed of O 2*p*, Hf 4*f*, and 5*d* states. It has four peaks denoted by *g*1, *g*2, *h*/*g*12, and *h*12. The *g* notation represents the bonding of O 2*p*–Hf 5*d*, whereas *h* represents antibonding of O 2*p*–Hf 5*d*. We confirm that the energy of the Hf^1 interaction with O is lower than that of the Hf^2 interaction. The calculated net charges are −1.40 for O, 3.24 for Hf^1, and 3.15 for Hf^2. The overlap populations are 0.001 for the O–Hf^1 bond and 0.03 for the O–Hf^2 bond. The O–Hf^1 bond has a stronger ionic characteristic than the O–Hf^2 bond. The bonding character of the amorphous Hf-oxide thin films is different from that of the amorphous Zr-oxide thin films.

Figures 3(a) and (b) show the XANES spectra and the calculated O *K* edge of the amorphous Zr-oxide and Hf-oxide thin films. The difference between the measured XANES and the calculated O *K* edge obtained by a DV-$X\alpha$ and FLAPW methods is due to the mixture of the amorphous and crystalline phases of Zr oxide and Hf oxide in the thin

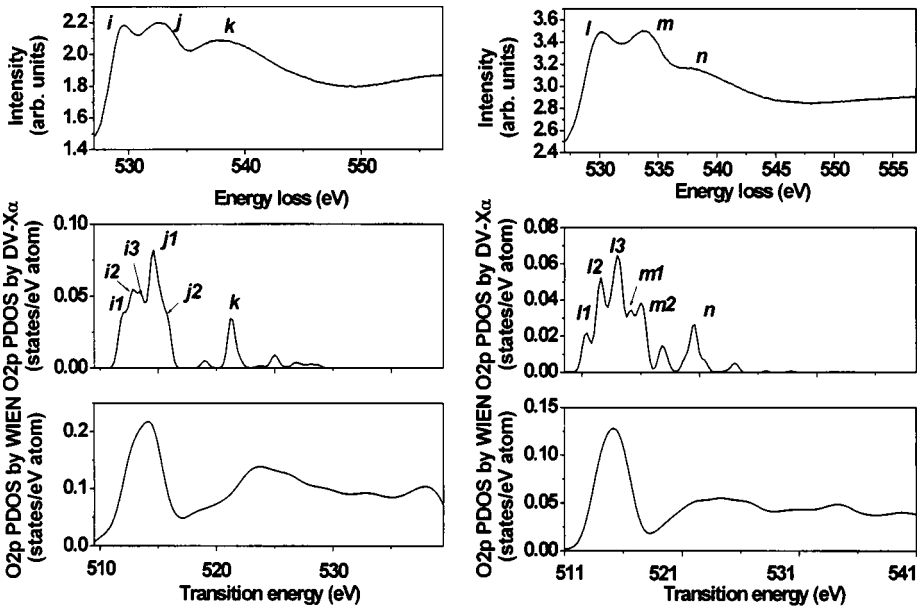

FIG. 3. Comparison of the experimental O *K* edge XANES and O *K* edge PDOS of (a) amorphous Zr-oxide thin films and (b) Hf-oxide thin films; Top: the experimental O *K* edge; Middle: the O 2*p* PDOS calculation based on the discrete variational $X\alpha$ method; Bottom: the O 2*p* PDOS calculation based on the linearized augmented-plane-wave method.

films.[12] The measured spectra for energies up to 20 eV above the edge reveal three peaks: *i*, *j*, and *k* for the Zr-oxide thin film and *l*, *m*, and *n* for the Hf-oxide thin film. The absolute transition energies of our calculations agree with the experimental results within an error of 10 eV, which is less than 2%.

We can understand the spectral features of the O *K* edge in the XANES results only by investigating the covalent interaction between O–Zr and O–Hf. The dominant components of the orbitals in the pertinent energy range are Zr 4*d*, 5*s*, and 5*p* states in the Zr-oxide thin films and Hf 5*d*, 6*s*, and 6*p* states in the Hf-oxide thin films. The O 2*p* state is a minor component made predominantly by the bonding interaction of Zr 4*d*5*sp* and Hf 5*d*6*sp*. Figures 4(a) and 4(b) show the DOS with overlap population diagrams for the $O-Zr^1$ and $O-Zr^2$ bonds of the Zr-oxide thin films and the $O-Hf^1$ and $O-Hf^2$ bonds of the Hf oxide thin films.

Peak *i* and peak *j* in Fig. 3(a) can be divided into groups of three and two subpeaks based on the origin of peaks: *i*1, *i*2, and *i*3; *j*1 and *j*2. The dominant components are Zr^2 4*d* for peak *i*, Zr^1 4*d* for peak *j*, and $Zr^{1,2}$ 5*s* for peak *k* [Fig. 4(a)]. This means that Zr^2 4*d* interact with O 2*p* within 3 eV above the edge, and Zr^1 4*d* interacts with O 2*p* at energies over 3 eV above the edge. The Zr 4*d*–Zr 4*d* interaction causes the splitting of the peaks into *i*1, *i*2, and *i*3 and into *j*1 and *j*2 [Fig. 5(a)]. Peak *i*1 and peak *i*2 signify the bonding and antibonding of Zr^2 4*d*–Zr^2 4*d*; peak *i*3 signifies the bonding of Zr^2 4*d*–Zr^2 4*d* and the antibonding of Zr^1 4*d*–Zr^1 4*d*. Peak *j*1 signifies the bonding of Zr^1 4*d*–Zr^1 4*d*, and peak *j*2 signifies the antibonding of Zr^1 4*d*–Zr^1 4*d*. We confirmed that exciting electrons from O 2*p* to Zr^2 4*d* cause a direct transition within 3 eV transition within 3 eV above the absorption edge, and that exciting electrons from O 2*p* to Zr^1 4*d* cause a direct transition at energies over 3 eV above the edge.

Peak *l* and peak *m* in Fig. 3(b) can be divided into

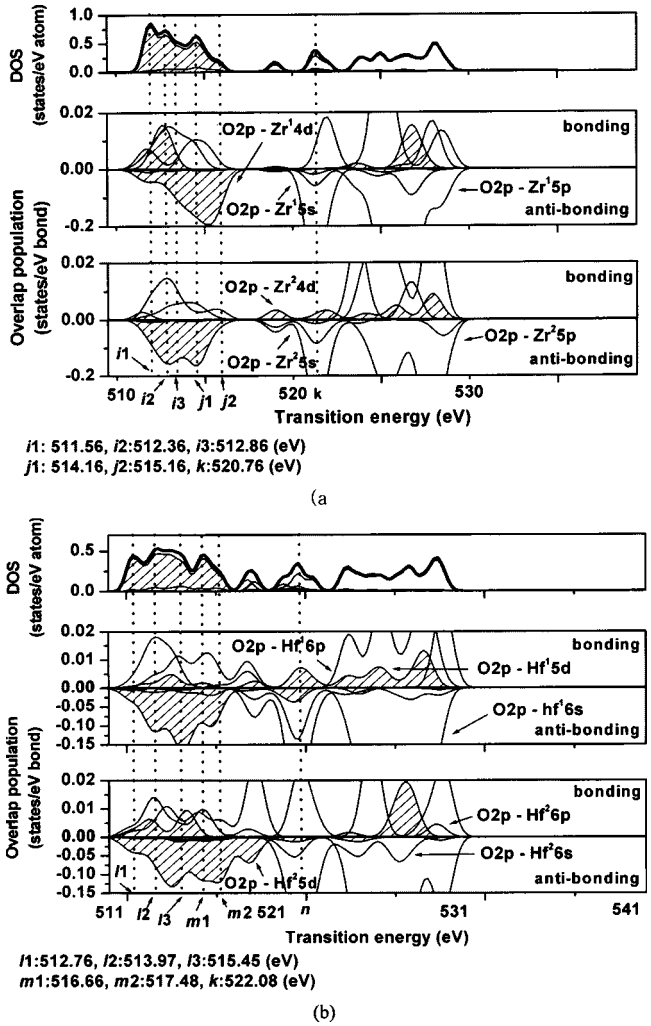

FIG. 4. Density of states (top), bond-overlap population diagrams (middle) for $O-Zr^1$ and $O-Hf^1$ bonds, and bond-overlap population diagrams (bottom) of $O-Zr^2$ and $O-Hf^2$ bonds.

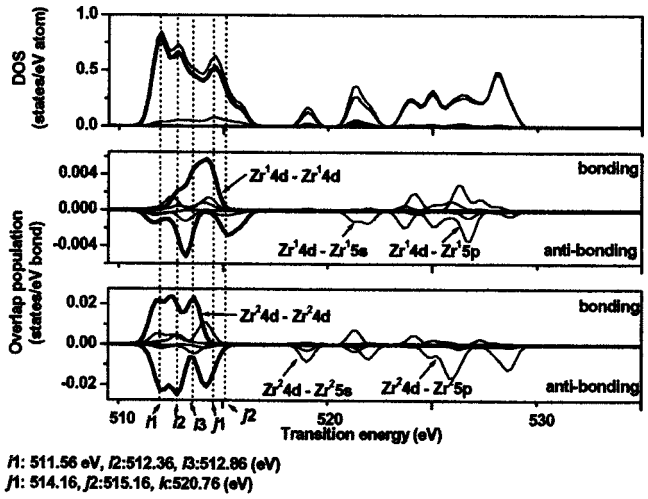

(a)

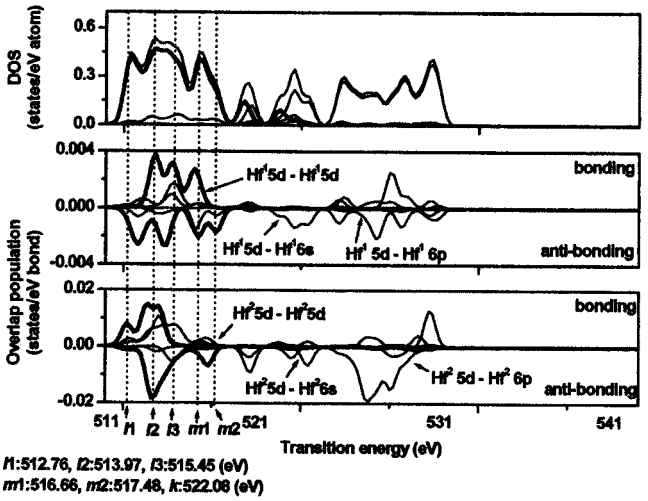

(b)

FIG. 5. Density of states (top), bond-overlap population diagrams (middle) for Zr^1-Zr^1 and Hf^1-Hf^1 bonds, and bonds-overlap population diagrams (bottom) of Zr^2-Zr^2 and Hf^2-Hf^2 bonds.

groups of three and two subpeaks based on the origin of peaks: $l1$, $l2$, and $l3$; $m1$ and $m2$. The dominant components are Hf^1 $5d$ for peak l, Hf^2 $5d$ for peak m, and $Hf^{1,2}$ $6sp$ for peak n [Fig. 4(b)]. In a range of 4 eV above the absorption edge, O $2p$ interact with Hf^1 $5d$ and Hf^2 $5d$ together, but the interaction of O $2p$ and Hf^1 $5d$ is stronger. At energies over 4 eV above the edge, O $2p$ interacts with Hf^2 $5d$. The Hf $5d-$Hf $5d$ interaction causes the splitting of the peaks into $l1$, $l2$, $l3$; $m1$ and $m2$ [Fig. 5(b)]. Peak $l1$ signifies the antibonding of Hf^1 $5d-Hf^1$ $5d$; peak $l2$ signifies the bonding of Hf^1 $5d-Hf^1$ $5d$ and the antibonding of Hf^2 $5d-Hf^2$ $5d$; peak $l3$ signifies the bonding of Hf^1 $5d-Hf^1$ $5d$. Peak $m1$ signifies the bonding and antibonding of Hf^1 $5d$ and Hf^1 $5d$; peak $m2$, the antibonding of Hf^2 $5d$ and Hf^2 $5d$. From these results, we confirm that the excitation of electrons from O $2p$ to Hf^2 $5d$ causes a direct transition within a range of 4 eV above the absorption edge, and that excitation of electrons from O $2p$ to Hf^1 $5d$ cause a direct transition at energies over 4 eV above the edge.

IV. CONCLUSIONS

We used first-principles calculations to investigate the electronic structure and transition states of amorphous Zr-oxide and Hf-oxide thin films. In modeling, $(Zr_4O_{17})^{-18}$ and $(Hf_4O_{18})^{-20}$ cluster models with oxygen defects were selected for amorphous TM oxide thin films. In the electronic structure, we found that, depending on the bond environment, films have different ionic and covalent characteristics for the O–Zr and O–Hf bonds. In XANES analysis, it was confirmed that the direct transition mechanism differs in the two TM oxide thin films. The amorphous Zr-oxide thin films absorb light by exciting electrons from the O $2p$ state to the Zr^2 $4d$ state at low energies above E_g. The absorption by electrons from the O $2p$ state to the Zr^1 $4d$ state occurs at high energy. In contrast, the amorphous Hf-oxide thin films absorb light by exciting electrons from the O $2p$ state to the Hf^1 $5d$ state at low energies above E_g. The absorption by electrons from the O $2p$ state to the Hf^2 $5d$ state occurs at high energies.

ACKNOWLEDGMENTS

This work was supported by the Ministry of Education ("Brain Korea 21") and the Ministry of Science and Technology. The experiments at PLS were supported in part by MOST and POSCO.

[1] W. J. Qi, R. Nieh, B. H. Lee, L. G. Kang, Y. Jeon, and J. C. Lee, Appl. Phys. Lett. **77**, 3269 (2000).
[2] G. Wilk, R. W. Wallace, and J. M. Anthony, J. Appl. Phys. **89**, 5243 (2001).
[3] E. Kim, S. –Y. Moon, Y. –H. Kim, H. –S. Yoon, and K. No, Jpn. J. Appl. Phys., Part 1 **39**, 6321 (2000).
[4] S. K. Kim, M. A. Kang, J. M. Shon, S. H. Kim, and K. No, Opt. Mater. (Amsterdam, Neth.) **22**, 361 (2003).
[5] H. Adachi, M. Tsukada, and C. Satoko, J. Phys. Soc. Jpn. **45**, 875 (1978).
[6] D. E. Ellis, H. Adachi, and F. W. Averill, Surf. Sci. **58**, 497 (1976).
[7] J. P. Perdew, K. Burke, and M. Ernzerhof, Phys. Rev. Lett. **77**, 3865 (1996).
[8] J. Tauc *et al.*, Phys. Status Solidi A **15**, 527 (1996).
[9] P. Blaha, K. Schwarz, G. K. J. Madsen, D. Kvasnicka, and J. Luitz, WIEN: *An Augmented Plane Wave+Local Orbitals Program for Calculating Crystal Properties*, revised ed. (Technische Universitat WIEN, Austria, 2001).
[10] J. C. Slater, *Quantum Theory of Molecules and Solids* (McGraw-Hill, New York), Vol. 4.
[11] C. Hébert, J. Luitz, and P. Schattschneider, Micron **34**, 219 (2003).
[12] V. V. Roddatis, D. S. Su, E. Beckmanm, F. C. Jentoft, U. Braun, K. Krohnert, and R. Schlogl, Surf. Coat. Technol. **151**, 63 (2002).